

Variability of the proton-to-electron mass ratio on cosmological scales

Critical examination of positive detection

M.Wendt^{1,a} and D.Reimers¹

Hamburger Sternwarte, Universitat Hamburg, Gojenbergsweg 112, 21209 Hamburg, Germany

Abstract. The search for a possible variation of fundamental physical constants is newsworthy more than ever. A multitude of methods were developed. So far the only seemingly significant detection exists for the proton-to-electron mass ratio as stated by Reinhold *et al.* [1]. The positive detection is based on the combined analysis of H₂ absorption systems in the spectra of Q0405-443 and Q0347-383 at $z_{\text{abs}} = 2.595$ and $z_{\text{abs}} = 3.025$, respectively. The high resolution data of the latter is reanalyzed in this work to examine the influence of different fitting procedures and further potential nonconformities. This analysis cannot reproduce the significance achieved by the previous detection.

1 Introduction

Contemporary theories of fundamental interactions, particularly those subsumed as string theories allow for all kinds of variations of fundamental constants in the course of the evolution of the universe. Variations of the coupling constants of strong and electroweak interactions would affect the masses of elementary particles dependent on the model for the expanding universe. It is up to cosmology to achieve first estimates and constraints of possible variations on large scale since laboratory experiments lack the spatial or temporal coverage. A recent analysis of HE 0515-4414 by Chand *et al.* [2] and Molaro *et al.* [3] yielded a result for the fine structure constant that is in good agreement with no variation at the current level of accuracy. A claimed detection of significant positive variation in the proton-to-electron mass ratio [4] and a later refinement to $\Delta\mu/\mu = (2.0 \pm 0.6) \times 10^{-5}$ [1] launched numerous theories with different scenarios to interpret the new data. The subject is still under heavy debate and confirmation of the results and methods is required.

2 Detecting $\Delta\mu/\mu$ via molecular hydrogen

The latest measured value of the proton-to-electron mass ratio is $\mu_0 = 1836.15267261(85)$ [6]. The precision reached by today's laboratory experiments rules out considerable variation of μ on short time scales but cannot yet exclude a change over cosmological timescales on the order of 10^{10} years. Additionally the possibility of different proton-to-electron mass ratios in widely separated regions of the universe cannot be rejected. The method to constrain a possible variation of μ as applied in this work was first suggested by Varshalovich and Levshakov [5]. Electronic, vibrational, and rotational excitations of a diatomic molecule depend differently on its reduced mass μ . To a first approximation, these energies are proportional to μ^0 , $\mu^{-\frac{1}{2}}$, μ^{-1} ,

^a e-mail: mwendt@hs.uni-hamburg.de

respectively. Hence each transition has an individual sensitivity to a possible change in that reduced mass. This can be expressed by a sensitivity coefficient.

$$K_i = \frac{d \ln \lambda_i}{d \ln \mu} = \frac{\mu}{\lambda_i} \frac{d \lambda_i}{d \mu}. \quad (1)$$

The calculations of K_i were recently refined by Reinhold *et al.* [1]. In first order they can be expressed by the Dunham coefficients Y_{kl} of the ground and excited states. With $\mu_n = \frac{m_e \mu}{2}$, Equation 1 leads to:

$$K_i = -\frac{\mu_n}{\lambda_i} \frac{d \lambda_i}{d \mu_n} = \frac{1}{E_e - E_g} \left(-\frac{\mu_n d E_e}{d \mu_n} + \frac{\mu_n d E_g}{d \mu_n} \right). \quad (2)$$

The computations for the energies of the excited and ground state, E_e and E_g , respectively are the same as for the energy levels of H_2 . Starting with the BOA based on the semiempirical approach the energy levels can be expressed by the Dunham formula

$$E(v, J) = \sum_{k,l} Y_{kl} \left(v + \frac{1}{2} \right)^k [J(J+1) - A^2]^l; \quad A^2 = 0 \quad (\text{Lyman}), 1 \quad (\text{Werner}) \quad (3)$$

However, the Dunham coefficients Y_{kl} cannot be calculated directly from the level energies due to strong mutual interaction between the excited states as well as avoided rotational transitions between nearby vibrational levels. For the first time the more complex non-BOA effects are taken into account in the work of Reinhold *et al.* [1]. Their recent precise laboratory measurements of the level energies of molecular hydrogen allowed for a reliable enhancement of the BOA approximation. The influence of the inclusion of the Bohr shift and adiabatic corrections is shown in Figure 1 (*right*) in percentage compared to prior sensitivity coefficients [7].

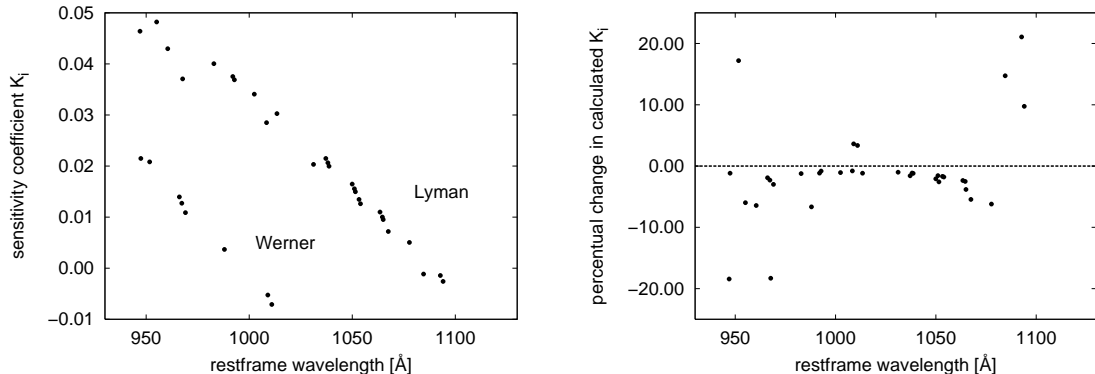


Fig. 1. Sensitivity coefficients of observed lines in the Lyman and Werner band (*left*) and recent refinement of K_i given in percentages (*right*).

2.1 Distinguish cosmological redshifts from variation of μ

With K_i from Equation 1, the rest frame wavelengths λ_i^0 are related to those in the quasar absorption system λ_i via

$$\lambda_i = \lambda_i^0 \left(1 + z_{\text{abs}} \right) \left(1 + K_i \frac{\Delta \mu}{\mu} \right), \quad (4)$$

with z_{abs} as the redshift of the absorbing system. This can be expressed in terms of the individual redshift of each measured H_2 component:

$$z_i = z_{\text{abs}} + bK_i. \quad (5)$$

According to Equation 5 the redshift of each H_2 feature can be distinguished between the intrinsic redshift of the absorber and an additional component due to a possible variation in μ . Equation 5 describes a simple linear equation with a gradient of

$$b = (1 + z_{\text{abs}}) \frac{\Delta\mu}{\mu}. \quad (6)$$

A linear regression of the redshift of each H_2 line z_i and its individual sensitivity coefficient K_i will yield the redshift of the absorbing DLA system and $\Delta\mu/\mu$ during the epoch between $z = z_{\text{abs}}$ and today. It is worth noting that in the case of non-zero variation the redshift of the absorber is not identical to the mean redshift of all observed lines as can be derived from Equation 5.

3 Observations

The source (Q0347-383) of the analyzed spectrum is a bright quasi-stellar radio object (QSO) with a visual magnitude of $V = 17.3$ mag at a redshift of $z = 3.23$ [8]. The precise position dated to 2000 as stated in the fifth fundamental catalogue is $\alpha 03h 49m 43.68s$, $\delta -38^{\circ}10' 31.3''$. The Quasar absorption line spectra were obtained with the Ultraviolet and Visual Echelle Spectrograph (UVES) at the Very Large Telescope (VLT) of the European Southern Observatory (ESO) in Paranal, Chile. The slit was 0.8 arcsec wide resulting in a spectral resolution of $R \approx 53.000$ over the wavelength range $3300\text{\AA} - 4500\text{\AA}$.

The average seeing during observation was about 1.2 arcsec. Before and after the exposures for each night, Thorium-Argon calibration data were taken. An overall of nine spectra were recorded with an exposure time of 4500 seconds each between January 8th and January 10th 2002 for the ESO program 68.A-0106(A). All spectra were taken with grating 430 and the blue “Pavarotti”-CCD with 2x2 binning. Later on the data were reduced manually by Mirka Dessauges-Zavadsky from Geneva Observatory in Jan 2004 to achieve maximum accuracy. The ESO Ambient Conditions Database¹ includes measurements of the environmental parameters at the Paranal ESO observatory and shows no significant changes in temperatures during or in-between the exposures that could lead to shifts between the separate observations. The reduced data used here is identical to the one in [4] and [1].

4 Data analysis

The nine separate spectra are coadded only to identify H_2 lines with a higher signal-to-noise ratio. The fitting is carried out simultaneously on the separate spectra to avoid influences of slight shifts between the datasets. The observed spectral range of the data covers over 80 H_2 lines of which after careful selection and avoidance of blends only 39 are taken into account for the analysis. The H_2 lines are mostly noticeable by their narrow line profiles and generally low equivalent width. The observed spectrum has an instrumental resolution of 5.6 km s^{-1} . That corresponds to a temperature of more than 4000K for Doppler broadened H_2 lines. A lower excitation temperature is to be expected for intergalactic molecular Hydrogen. The observed width of the H_2 features can thus be expected to be given by the spectral resolution.

¹ <http://archive.eso.org/eso/ambient-database.html>

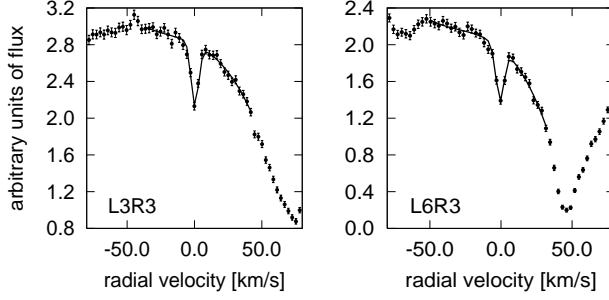


Fig. 2. Continuum matching via parabolic fit to the observed flux for L3R3 and L6R3.

4.1 Fitting of H₂ features

The selected and verified H₂ lines are fitted with an evolutionary fitting algorithm [9]. Due to the nature of DLA systems the continuum is heavily contaminated. The background is determined over a given range of the line feature and fitted with a polynomial. That range is selected individually for each line by eye to have the best compromise between a clean continuum and the number of pixels contributing to it. The grade of the polynomial is manually selected to match the continuum flux. In some cases an additional line is fitted along with the H₂ component to have a better fit to the flux. For those cases the true continuum is fitted via a linear function. In cases of a continuum flux with apparent influences of broad Lyman α features or general contamination, a parabolic or cubic function is used to fit the background to the observed flux. See Figure 2 of L3R3 and L6R3 for an exemplar of a parabolic fit.

This approach – however necessary – is highly critical. The applied rectification of the flux may have an impact on the fitted central position of the line feature. For the analysis in [1] and [4] the estimated background is constructed manually. To ascertain the validity of this approach a series of fits for simulated spectra is carried out. A spectrum of a hypothetical H₂ feature on the wing of a broad almost saturated HI absorption feature is synthesized. Its relative position to the center of the HI feature is altered to cover the full area of influence of the dominant atomic hydrogen feature. For each constellation 100 spectra are synthesized and fitted. Figure 3 (left) shows an example setup. For the given position of the H₂ feature the resulting error in determining the center of the H₂ absorption feature can be computed by the difference of the input to the artificially generated spectrum and the output of the fitting algorithm. On the *right* panel of Figure 3 the results of a full run of 10,000 fits are plotted. Figure 4 illustrates the averaged computed absolute error and the error as ascertained by the

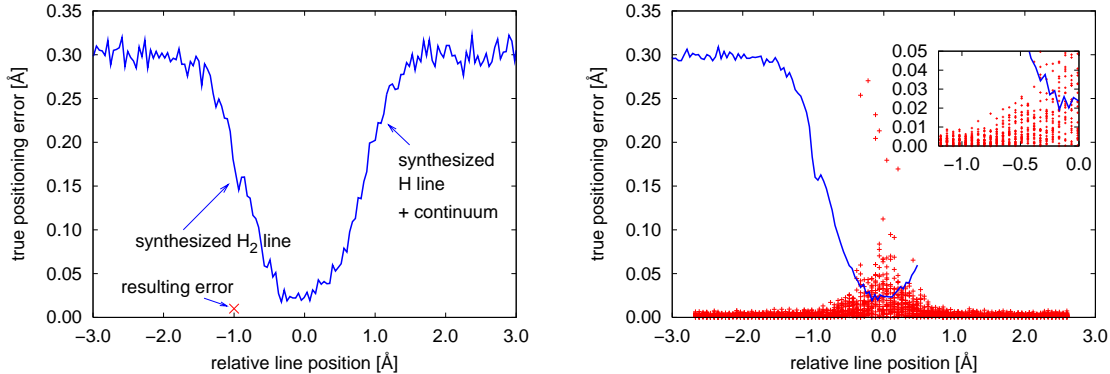


Fig. 3. Series of fits of synthesized spectra. On the left an exemplified case and on the right an overview with a blow up of the central region.

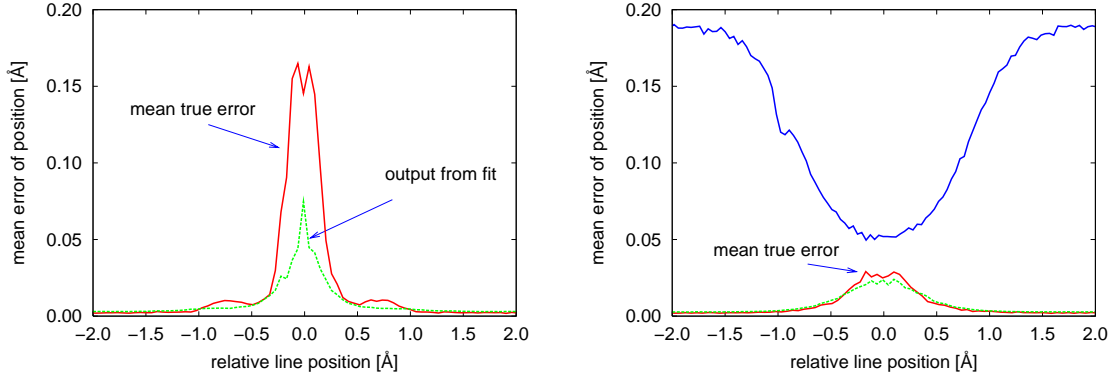


Fig. 4. Mean value of the true error and outcome of the fitting procedure. Comparison of the single component fit (*left*) and the two component fit (*right*).

fitting algorithm. To evaluate the accuracy of a polynomial continuum fit, two separate runs are carried out. One with a parabolic continuum fit (*left* panel) and one with a linear continuum but a second absorption line (in this case the broad HI line) as free parameter to match the observed flux (*right* panel). The latter representing the true physical conditions but not being feasible on heavily contaminated continua. The results indicate that modelling the pseudo continuum with a polynomial is valid when being performed carefully with respect to the underlying absorption. The error rises dramatically for positions near the center of the HI absorption which is understandable due to the low equivalent width of the H₂ feature. However in the case of the polynomial continuum fit this effect has greater influence. Furthermore the application of the polynomial fit to the continuum and accordingly the rectification of the flux introduces a net shift in the determination of the as seen in Figure 5. An error that may not average out for low statistics.

4.2 Selection of lines

The strong contamination of the observed spectrum forces us to find a balance between a sufficiently high number of H₂ features taken into account for better statistics and the quality of the surrounding continuum. An independent selection via curve of growth analysis yields the same group of H₂ lines as used in [1] and [4].

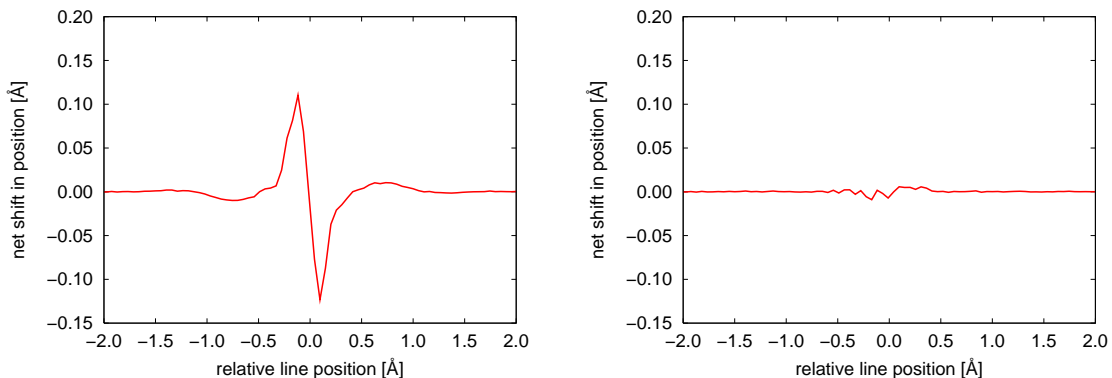


Fig. 5. Mean shifts of fitted position over a series of fits for the single component fit (*left*) and the two component fit (*right*).

5 Results

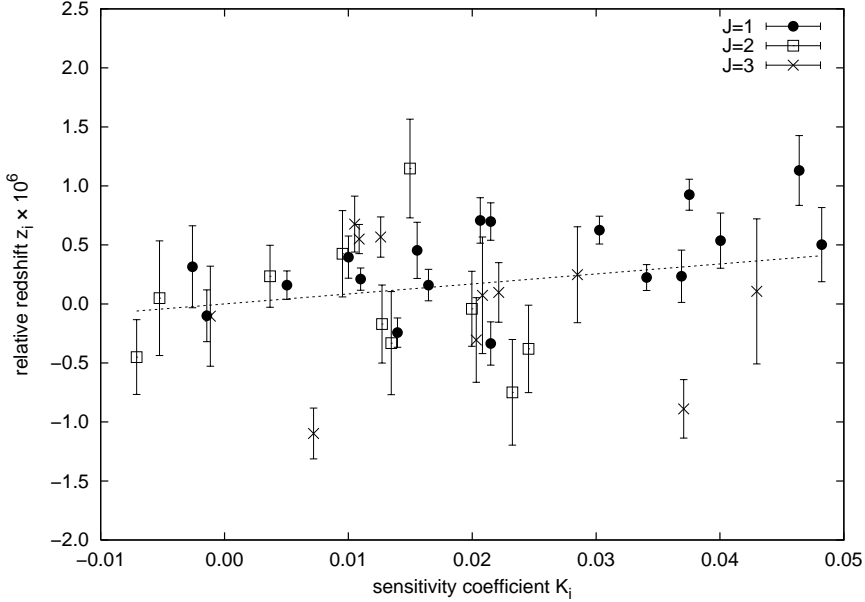


Fig. 6. Plot of $z_i - K_i$ relation for all observed rotational levels. The origin of the relative redshift corresponds to $z_{\text{abs}} = 3.024899$. The linear fit (dashed line) is consistent with $\Delta\mu/\mu = 2.1 \times 10^{-5}$.

All 39 lines are fitted and a corresponding redshift is derived. The measured redshifts with their obtained standard deviations are not consistent with a single mean redshift at the 1σ level. Accordant to the method described in Section 2 the measured redshifts are tested for a possible correlation with the individual sensitivity coefficients. Figure 6 shows the resulting plot. The dotted line represents a preliminary linear fit to the data. The redshift of the absorber does not correspond to the mean redshift, but can be ascertained by the point of zero sensitivity towards possible μ -variation, since at this point the measured redshift equals the cosmological redshift (see Eq. 5). The ordinate is given in relative redshift with respect to the absorber $z_{\text{abs}} = 3.0248990(13)$. The linear fit corresponding to $\Delta\mu/\mu = 2.1 \pm 1.4 \times 10^{-5}$ is achieved by a linear regression without taking into account the individual estimated errors in the redshift to allow for a comparison with the results of Reinhold *et al.* [1] who measured $\Delta\mu/\mu = 2.06 \pm 0.79 \times 10^{-5}$ with the method of an unweighted fit but based on a merged dataset of two quasars at different redshifts. The argumentation behind an unweighted fit is that the dispersion of the experimental points then characterizes the true statistical errors. At a 95% confidence level this results gives a constraint of the variation to $-0.7 \times 10^{-5} \leq \Delta\mu/\mu \leq 4.9 \times 10^{-5}$. However, a straight forward linear fit to the data turns out to be inappropriate.

Figure 7 illustrates the $z_i - K_i$ relation for all three observed rotational levels combined (*top left*) and each of them separately (*top right and bottom*). Evidently only the first rotational level shows an apparent correlation between redshift z_i and sensitivity coefficients K_i . Table 2 gives the mean redshifts \bar{z} for each corresponding rotational level. It is worth noting that the deviation $\sigma_{\bar{z}}$ from the mean value is smaller than the 2σ level of the mean estimated error $\bar{\sigma}_z$. The number of lines is too low to make significant statistical claims.

However, the Pearson product-moment correlation coefficient (equivalent to dividing the covariance between two variables by the product of their standard deviations) indicates only a very weak correlation of the data. Apparently only the first rotational level contributes to a positive linear correlation at all (see Table 1). A closer examination of the first rotational level (see Figure 7 *upper right*) by eye shows that the positive gradient of the linear regression seems

to evolve only by the rightmost seven data points. This impression can be confirmed by a correlation test for all data points except those seven lines with $J = 1$. Table 1 lists the correlation coefficient of this subset as $r = -0.08$. A result quite consistent with no correlation at all (see Fig.8). However, seven data points represent a considerable subset of the total of 39 lines. The seven lines (namely L7R1, L8R1, L9R1, L9P1, L10P1, L13R1, L14R1) evidently have a sensitivity coefficient of > 0.03 in common, they also emerge from high energy transitions. As can be seen from the line identifiers, the seven lines in question all arise from high vibrational levels in the Lyman band. This matches fully with the range where the sensitivity coefficients deviate the most from the Born-Oppenheimer-approximated calculations [1].

5.1 Goodness of fit

To quantify the z_i - K_i correlation further a Spearman rank-order correlation coefficient r_s is calculated. It is a non-parametric measure of correlation, i.e., it assesses how well an arbitrary monotonic function could describe the relationship between two variables without making any assumptions about the frequency distribution of the variables. Unlike the Pearson product-moment correlation coefficient, it does not require the assumption that the relationship between the variables is linear nor does it require the variables to be measured on interval scales. Furthermore it allows to determine the significance of a non-zero correlation. Instead of measured values merely their ranks are compared. The analysis gives coefficients of $r_s = 0.17$ for the full set of lines and $r_s = 0.08$ for the subset of 32 lines (see Figure 8). The latter being not significant at the 99.9% level (i.e., in only 0.1% of all cases a non-zero correlation can be deduced from a correlation coefficient of 0.08) thus in full agreement with no correlation. The obtained Spearman rank-order correlation coefficients occur in case of zero-correlation with probabilities of $\sim 1/3$ and $2/3$, respectively.

The goodness of fit states how well a statistical model fits a set of observations in contrast to a general σ of a fit which only states the confidence of the fit. The χ^2 based fit allows for a statement on the quality or rather the likelihood of a fit in respect to the model. Due to the simplicity of the assumed model (see Eq.5) the relation between measured redshift and computed sensitivity coefficient is stringently linear in case of variation. In case of no variation the gradient would be zero but still fit the assumed linear model. As a consequence, any result must be consistent with a linear correlation between z_i and K_i independently of a possible variation. The performed simulations of linefits indicated that the fit error on the observed wavelength for each line and thus the error in the relative redshift as estimated by the fitting programme are reasonable. This, of course, depends also on the accuracy of the errors given in the observed data. The correctness of the errors in the spectral data can be crudely tested by the χ^2 value of a reasonably good fit. However, the χ^2 is influenced by the trueness of the error as well as the accuracy of the model. The mean value of all 351 fitted lines (39 lines in 9 spectra) is $\bar{\chi}^2 = 1.16$ with a more descriptive median of exactly 1.00. The mean χ^2 is expected to lie above the median due to the fact that for some absorption features the model of a single component is knowingly wrong and thus the flux is not fitted by the model for the whole evaluated range.

The goodness of fit for the fitted linear relation gives a likelihood of the fit of $\ll 0.1\%$. This strongly indicates that the errors in general are underestimated. A lowered likelihood can also

Table 1. Correlation coefficients for different datasets

rotational level	r	data points
1	0.29	18
2	-0.16	10
3	-0.62	11
all	0.24	39
subset	-0.08	32

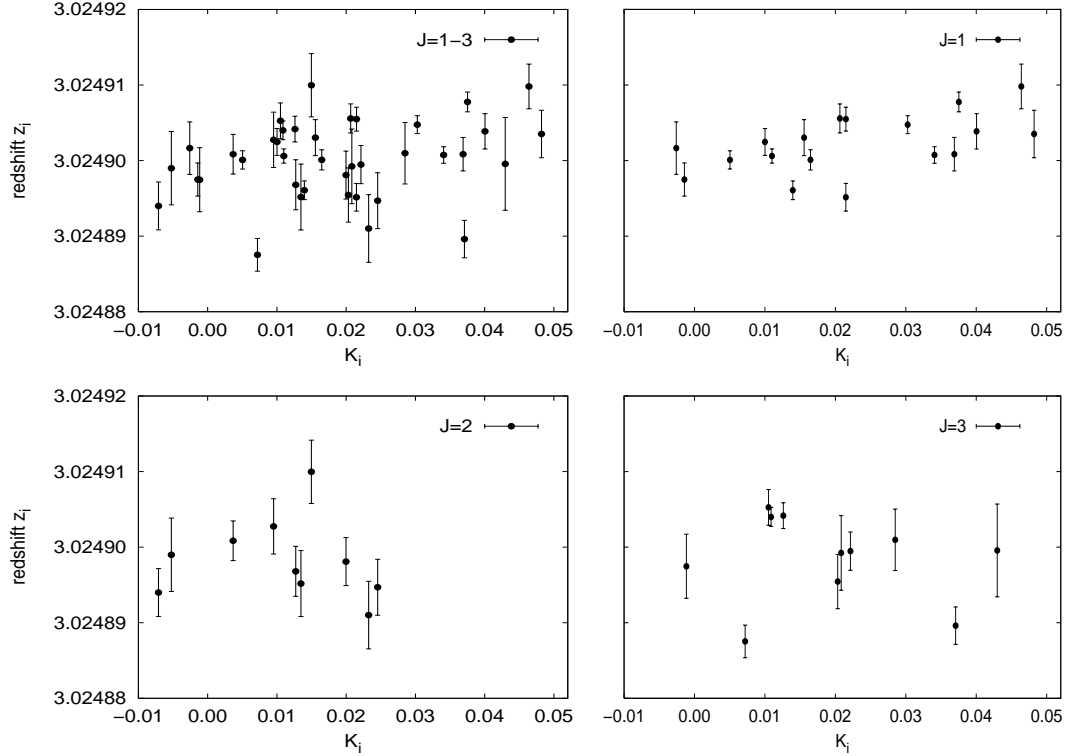


Fig. 7. $z_i - K_i$ relation with individual redshifts for the whole dataset (top left) and separate rotational levels $J=1$ to $J=3$ (top right and bottom).

emerge from measurement errors that are strongly non-normally distributed. The simulations with synthesized data, however, did show that the errors of the fit are in good agreement with a normal distribution for the lines selected. The validity of the assumed model is convincing and the errors of the fitted redshifts appear to be systematically underestimated. The fitted linear relation is not at all consistent with the observed data and the adopted error simply reflects the statistically best solution without considering consistency with the data. However, the likelihood of the fit scales rather strongly with the errors of the observed redshift. Assuming the greatest uncertainty in the measured redshifts despite the evidently accurate output of the fitting program, the errors given for the redshifts were scaled by a constant factor. A scaling by factor a factor of two results in a likelihood of the fitted data of about 25% which would be acceptable, though still being low.

Note, that for this analysis a constant shift or offset in wavelength calibration has no impact on the deduced correlation. Only differential shifts would influence the outcome of the analysis.

Table 2. The mean redshift \bar{z} for each rotational level, along with its standard deviation in comparison to the mean estimated error of the redshift $\bar{\sigma}_z$.

J	\bar{z}	$\sigma_{\bar{z}}$	$\bar{\sigma}_z$
1	3.0249022	3.8×10^{-6}	1.9×10^{-6}
2	3.0248982	5.3×10^{-6}	3.8×10^{-6}
3	3.0248984	5.7×10^{-6}	3.2×10^{-6}

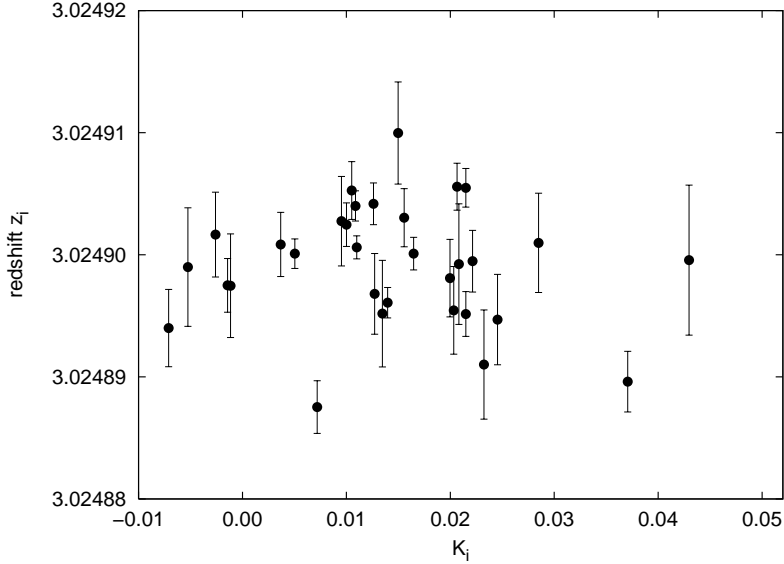


Fig. 8. $z_i - K_i$ relation with individual redshifts for the reduced dataset of 32 lines in all observed rotational levels. With a Spearman rank-order correlation coefficient of $r_s = 0.08$ the data is in distinct agreement with no correlation.

6 Conclusions

Asking for self consistency in the result, brings down the significance of the measurement of a possible variation to $\sim 1\sigma$ at once. Rejecting the subset of seven lines of a single rotational level from the dataset leads to no correlation at all, since the correlation is already very weak as discussed above. A linear fit is no longer reasonable. A detection of a positive variation of μ is caused solely from transitions for which $J = 1$ and $v > 7$ in the upper state, i.e., a range of transitions with significant non-BOA effects as reflected in the large changes in recently calculated K_i or λ_i for these vibrational bands. The discrepancy of the observed redshifts and their errors with the basic model of $\lambda_{\text{obs}} = \lambda_0 \times (z_{\text{abs}} + 1)$ points out yet not fully understood systematic errors. Possible reasons for the scatter in the redshift of several σ can be that a resolution of 53.000 is not sufficient for accurate linefits of unresolved H₂ features and thus the positioning error is systematically underestimated.

A possible cause for differences in measured redshifts between the excitation levels can also be a spatial separation between the points of origin. The nature of DLAs is not yet fully understood and subject to several inconsistencies. Recent simulations indicate that molecular hydrogen is distributed highly inhomogeneous and clumpy [10]. Despite the successful refinement of transition frequencies for H₂ their accuracy for intergalactic physical conditions requires further verification. The yet unknown origin of the scatter of measures redshift in this work and others demands great care in future analysis and renders the gain in significance by combining data of several systems questionable. It would rather indicate the need for more careful selection of analyzed features, an in-depth study of the according transition wavelengths as well as a high precision reduction of the observed data in all particular steps (i.e. the data acquisition itself, wavelength calibration across several orders, vacuum correction). The level at which possible variations are investigated today sets high demands on all steps involved.

A possible variation of the proton-to-electron mass ratio cannot be confirmed. Furthermore the inconsistency of the data and the errors with respect to the scattering of the observed redshifts give reason to be more careful in formulating constraints as well.

The resulting constraint of this work at the 95% level is $|\Delta\mu/\mu| \leq 4.9 \times 10^{-5}$ over the period of ~ 11.5 Gyr, or a decrease of 4.3×10^{-15} yr⁻¹ for the hypothetical case of linear variation

in time. The *light travel time* of 11.496 Gyr for $z = 3.025$ corresponds to the cosmological parameters $H_0 = 71 \text{ km s}^{-1}\text{Mpc}^{-1}$, $\Omega_M = 0.27$, $\Omega_{\text{vac}} = 0.73$.

7 Acknowledgements

We are thankful for the support from the Collaborative Research Centre 676.

References

1. E. Reinhold *et al.*, Physical Review Letters **96**, (2006)
2. H. Chand *et al.*, A&A **451**, (2006) 45-56
3. P. Molaro *et al.*, A&A **712**, (2007)
4. A. Ivanchik *et al.*, A&A **440**, (2006) 45-52
5. D. A. Varshalovich and S. A. Levshakov, JETPL **58**, (1993) 237-240
6. P. J. Mohr and B. N. Taylor, Reviews of Modern Physics **77**, (2005) 1-107
7. D. A. Varshalovich and A. Y. Potekhin, Space Science Reviews **74**, (1995) 259-268
8. D. Maoz *et al.*, ApJ **409**, (1993) 28-41
9. R. Quast, R. Baade and D. Reimers, A&A **431**, (2005) 1167-1175
10. H. Hirashita, A. Ferrara, K. Wada, P. Richter, MNRAS **18**, (2003) 341